Preprint
UCRL-JC-137307

High Temperature, High Strain Rate Extrusion of Ultrahigh-Carbon Steels

D. R. Lesuer, C. K. Syn, O. D. Sherby

This article was submitted to THERMEC-2000, Las Vegas, Nevada, December 4 – 8, 2000

August 23, 2000

U.S. Department of Energy

Lawrence
Livermore
National
Laboratory

This work was performed under the auspices of the United States Department of Energy by the University of California, Lawrence Livermore National Laboratory under contract No. W-7405-Eng-48.

High Temperature, High Strain Rate Extrusion of Ultrahigh-carbon Steels

D.R. Lesuer*, C.K. Syn*, O.D. Sherby**

** Lawrence Livermore National Laboratory, Livermore, CA 94551, USA*
*** Dept. of Materials Science and Eng., Stanford University, Stanford, CA 94305, USA*

Abstract

It is shown that high rate extrusion is a viable production process for obtaining desirable microstructures and mechanical properties in ultrahigh carbon steels (UHCSs). The coefficient of friction for extrusion was determined for the UHCSs as well as five other materials and shown to be a function of stress - decreasing with increasing stress. The extruded UHCSs deform by a diffusion-controlled dislocation creep process. Stacking fault energies have been calculated from the extrusion data and observed to decrease with increasing concentrations of silicon, aluminum and chromium. Microstructures are either ultrafine pearlite when extruded above the eutectoid temperature or ultrafine spheroidite when extruded below the eutectoid temperature. The resulting strength - ductility properties are shown to be superior to those obtained in high-strength low alloy steels.

Keywords: Extrusion, Ultrahigh Carbon Steels, Creep, Friction Coefficient

1. Introduction

Ultrahigh-carbon steels (UHCS) containing 1 – 2.1% C are an emerging class of steel with high ambient-temperature strength, hardness, wear resistance and ductility [1]. Achieving good strength with high ductility requires microstructures containing ultrafine carbides in spherical or pearlitic form and the elimination of deleterious proeutectoid carbide networks. Many processing routes have been developed for producing these microstructures including hot and warm working, a divorced eutectoid transformation (DET), and a DET with associated deformation (DETWAD) [1]. However, these processing routes are a significant departure from current steel processing practice and thus less likely to be adopted in commercial application. Recently, extrusion has been examined as a single-step thermo-mechanical process for UHCS [2]. In this recent study, the microstructure-property relations were examined for UHCS, which was hot extruded in the single-phase austenite region and in the two-phase austenite + carbide region without any subsequent heat treatment. The results showed that, depending on steel composition and extrusion temperature, grain boundary carbide networks and graphite could be avoided. In addition, excellent combinations of strength and ductility were obtained, which were superior to the properties that could be obtained with conventional low carbon steels, conventional high strength steels and dual phase steels. In this paper, additional insight into the high temperature ($0.6 - 0.9T_m$), high strain rate ($1.4\ s^{-1}$) extrusion of UHCS is provided. The pressure – time history of the extruded billets is analyzed to determine the strain rate – stress response of the materials and the coefficients of friction during extrusion are evaluated. Atomic diffusion, elastic modulus and stacking fault energy are known to contribute to the flow stress and strain rates during extrusion and thus the influence of these material characteristics on the constitutive response are examined. The resulting

microstructures and the influence of extrusion temperature on the ambient-temperature stress–strain behavior are then studied.

2. Materials

Four UHCSs were used in this study. The chemical composition and alloy designation for these materials are shown in Table 1. The materials were extruded at three temperatures, 900, 1025 and 1150°C, and air cooled. At these temperatures, the alloys were either in the austenite range or the austenite + carbide range. Extrusion was done through round dies using a nominal 16:1 reduction ratio at an average effective strain rate of 1.4 s^{-1}. Further details concerning the thermomechanical processing and extrusion of these materials can be found in reference [3].

Table 1. Chemical composition of UHCS materials studied.

Alloy Designation	Composition, wt%
UHCS-1.30C-0.5Si	1.30C, 0.5Si, 0.5Mn, Balance Fe
UHCS-1.23C-1.2Si	1.23C, 1.2Si, 0.5Mn, Balance Fe
UHCS-1.15C-1.6Al	1.15C, 1.6Al, 0.5Mn, Balance Fe
UHCS-1.80C-1.6Al-1.5Cr	1.80C, 1.6Al, 0.5Mn, 1.5Cr, Balance Fe.

3. Coefficients of friction

The extrusion experiments were conducted on UHCS alloys that were contained within a mild steel can. Analysis of the extrusion data to obtain the flow stress of the UHCSs was based on pressure-time records and the measured external strain rate. The coefficient of friction (Ψ) during extrusion can be calculated as defined in Eq. (1),

$$\Psi = \sigma_{eff} / \sigma_{ext} \quad (1)$$

where σ_{eff} is the effective stress for frictionless deformation of the materials and σ_{ext} is the flow stress of the material during extrusion. The quantity σ_{ext}, which includes friction, can be calculated from the expression $\sigma_{ext} = P/\ln(A_o/A)$, where P is the steady-state pressure during extrusion, A_o is the initial area of the extrusion and A is the final area. Flow stress data in torsion were available for two of the UHCSs (UHCS-1.30C-0.5Si and UHCS-1.80C-1.6Al-1.5Cr) and for the mild steel can. Thus, assuming isostrain behavior, σ_{eff} for these extruded materials could be calculated. The average value of Ψ for these UHCS-based materials at the three temperatures of extrusion was 0.38. The details of the calculations have been provided by Lesuer et al. in ref. [3].

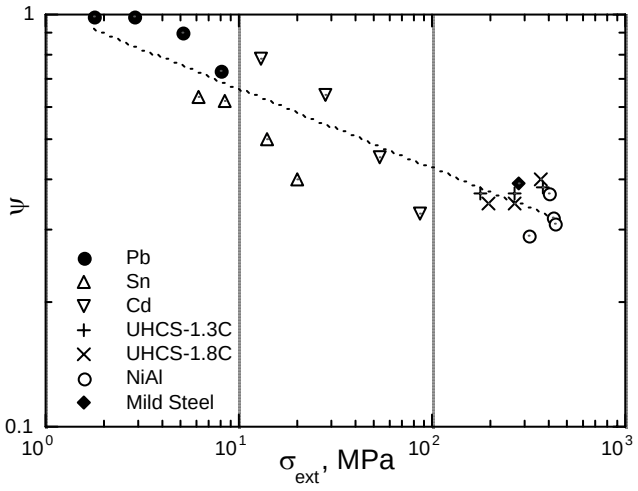

Fig. 1. Influence of flow stress of extrusion on the coefficient of friction for UHCS-1.30C-0.5C and UHCS-1.8C-1.6Al-1.5Cr and five other materials.

The values of Ψ have also been calculated for Pb, Sn, Cd, mild steel and NiAl from literature data on creep and extrusion flow stresses. The results are plotted in Fig. 1 as a function of σ_{ext} on logarithmic scales. Also included in the figure are the friction coefficients for the UHCS materials. The results in Fig. 1 show that the Ψ decreases as σ_{ext} increases; thus friction is providing an increasing contribution to σ_{ext} (and the energy required for extrusion) as σ_{ext} increases. In addition, the results in Fig. 1 suggest a power law relationship between Ψ and σ_{ext}. This power-law relationship provides a useful guide to obtain values of Ψ for materials/extrusion conditions for which coefficients of extrusion are unknown. Previous work by the authors [3] suggests that the decrease in Ψ with increase in σ_{ext} could be related to the unique state of stress during extrusion or to accompanying microstructural changes.

4. Constitutive response

Given the friction coefficient and the observation of isostrain behavior, the steady state, effective strain rate - effective flow stress response of the UHCS materials in Table 1 were determined. The effective strain rate was calculated as the time average strain rate for a volume element moving through the die using relationships developed by Jonas and Chandra [4]. In Fig. 2, the lattice-diffusion compensated strain rate is plotted as a function of the modulus-compensated flow stress for the four UHCS materials studied. In the graph a creep datum point for pure iron is included as well as creep data for an austenitic stainless steel. Pure iron and austenitic stainless steel are representative of high and low stacking fault energy materials respectively.

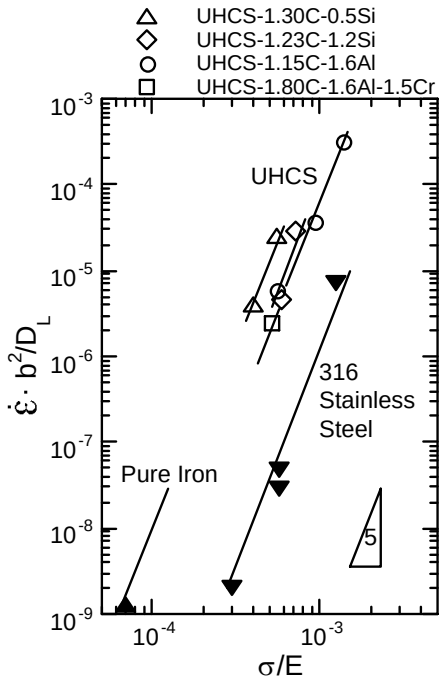

Fig. 2. Lattice-diffusion compensated strain rate as a function of modulus-compensated stess for the UHCS materials, pure iron and stainless steel. All materials were deformed in the

The slope of the curves for the austenitic UHCS materials is about five. This variation of strain rate with stress suggests that the dominant deformation resistance is diffusion-controlled dislocation creep [5, 6], which can be described by the following constitutive equation,

$$\dot{\varepsilon} = A^* \cdot (D_L/b^2) \cdot (\sigma/E)^5 \qquad (2)$$

where A* is a constant for a given material, D_L is the lattice self-diffusion coefficient, b is the magnitude of the burgers vector and E is the dynamic unrelaxed elastic modulus.

In Fig. 3(a), the strain rate – stress response derived from the extrusion experiments of Fe-1.3C-0.5Si alloy is compared with the response of the same alloy during torsion experiments [7]. Data is provided over a range of temperatures (750-1200°C) and strain rates (0.2 - 26 s^{-1}). The microstructures for the samples tested at 1000 to 1200°C consisted of all austenite, while the microstructures for the samples tested at 750°C and 900°C consisted of austenite and some cementite. The data in Fig. 3(a) has a stress exponent of 5 consistent with Eq. (2).

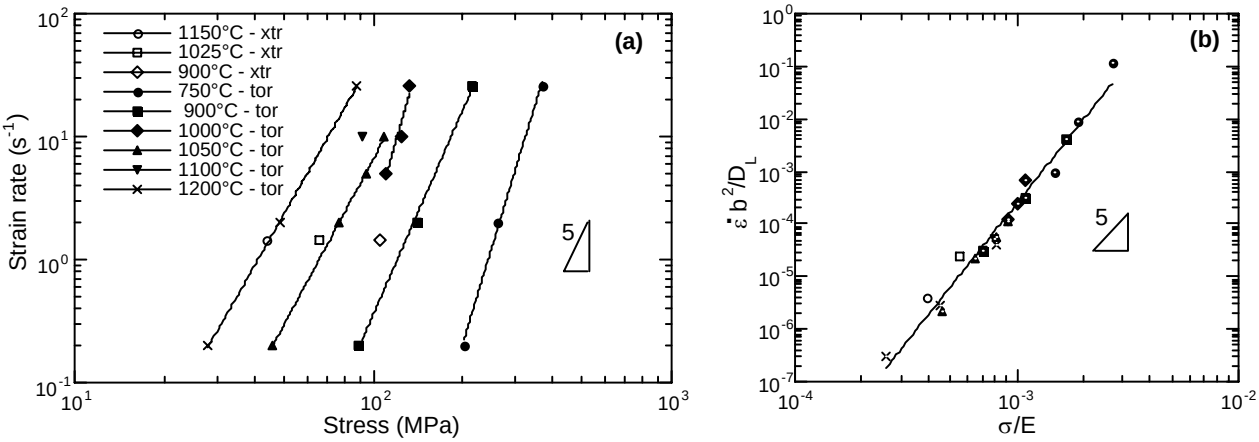

Fig. 3. Torsion (tor) and extrusion (xtr) data for the Fe-1.3C-0.5Si alloy obtained at a range of strain rates. The strain rate – stress behavior is shown in (a). The data has been re-plotted as $\dot{\varepsilon}b^2/D_L$ versus σ/E in (b).

The data in Fig. 3(a) is re-plotted as $\dot{\varepsilon}b^2/D_L$ versus σ/E in Fig. 3(b). For this analysis, the self diffusion coefficient of iron in austenite (D_L) was taken from the work of Mead and Birchenall [8], who studied self-diffusion in austenite as a function of carbon concentration. The values of E were taken as a function of temperature from the dynamic elastic moduli obtained by Andrews [9]. All the data in Fig. 3(b) fall along a single straight line with very little scatter. This excellent correlation is particularly impressive given the range of temperatures and strain rates and the fact that the microstructures at the two lowest temperatures (750°C and 900°C) contained austenite and cementite. The results confirm that the dominant deformation resistance at these high temperatures (~0.6 - 0.9 T_m) and high strain rates (~1 - 100 s^{-1}) is climb-controlled dislocation creep.

5. Influence of stacking fault energy

The data in Fig. 2 can be used to predict the stacking fault energy (γ) for the UHCS materials. The predictions are based on the well-established power-law relationship between γ and A*. Using the experimentally-derived γ and A* values for austenitic stainless steel as a baseline, the γ for UHCS can be predicted from the A* values obtained from creep or extrusion experiments. The results are plotted in Fig. 4, where A* is plotted as a function of γ. The correlation is rather remarkable inasmuch as there is a very systematic variation of γ with increasing solid solution alloy additions. For pure iron, the predicted value is 250 mJ/m^2 decreasing only slightly for the 0.5%Si UHCS material (γ=200 mJ/m^2). The lowest deduced value of γ among the UHCS materials was for UHCS containing 1.6Al and 1.5Cr at about 100 mJ/m^2. These predictions, although realistic, await experimental studies since no values of γ have been

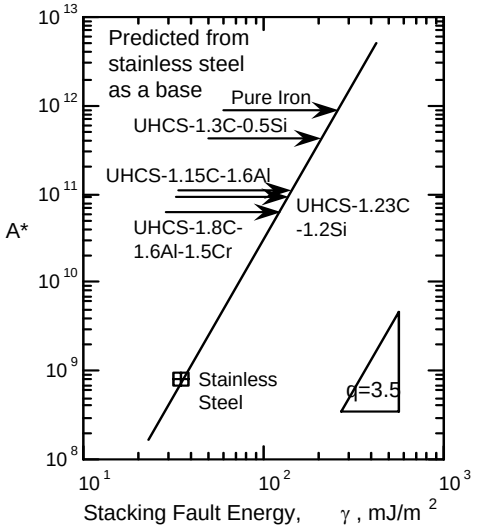

Fig. 4. Prediction of stacking fault energy of the UHCS alloys and pure iron using stainless steel as a baseline.

reported for pure iron or for iron-carbon alloys in the austenite range. In the analyses on solid solution alloying effects, the possible influence of 0.5% manganese, listed in Table 1, was not taken into account. It is assumed that this element is so similar to iron in atom size that it did not contribute to the strength of the UHCS materials.

6. Resulting microstructures and properties

Previous studies on the as-extruded and air-cooled bars showed that the UHCSs had high strengths at room temperature [2]. These high strengths were related to the fine pearlitic structures that were created during air-cooling from the extrusion temperature. Typical microstructures are shown for the as-extruded UHCS-1.2C-1.2Si in Fig. 5. A low magnification photomicrograph is shown in Fig. 5(a) where an outline of the prior austenite grain boundaries is given, showing a typical grain size of 150 μm. The mottled appearance of the outlined grains is related to pearlite colonies. These pearlite colonies are readily resolved with the scanning electron microscope and Fig. 5(b) shows the structure at a twenty-fold increase in magnification over that used in Fig. 5(a). Here, the pearlite, consisting of alternating plates of nearly pure iron and iron carbide, are within colonies of the order of 10 to 20 μm. These colonies are probably related to the subgrains that were created during deformation by extrusion. Such microstructural studies permitted the present authors to relate the room temperature strength of the UHCSs to the corresponding microstructure [2]. The closer the interplate spacing, the stronger the material.

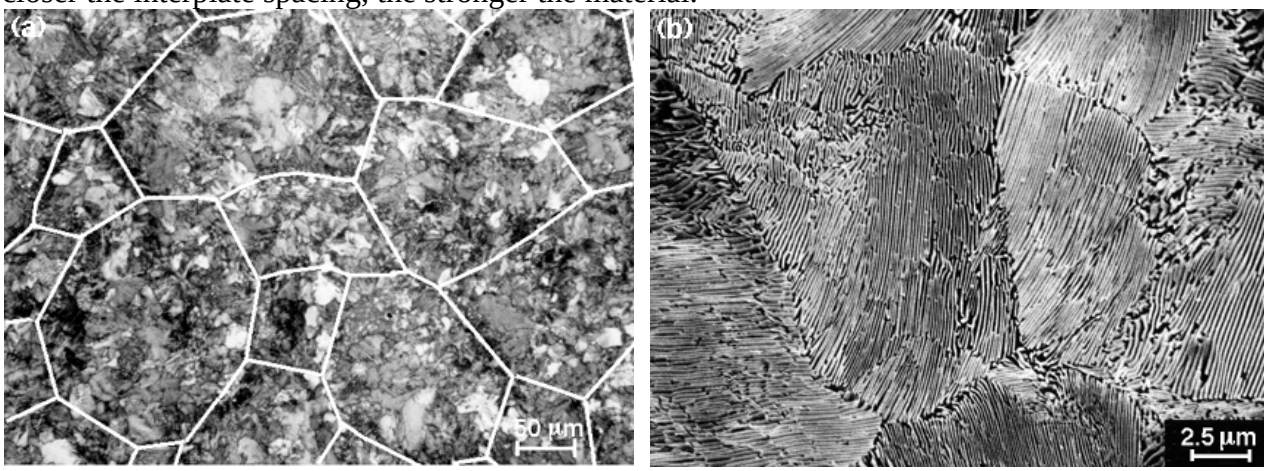

Fig. 5. Microstructures of UHCS-1.23C-1.2Si after extrusion at 1150°C and air cool. Prior austenite grain boundaries are outlined in optical micrograph (a) and pearlite colonies are clearly visible in SEM micrograph (b).

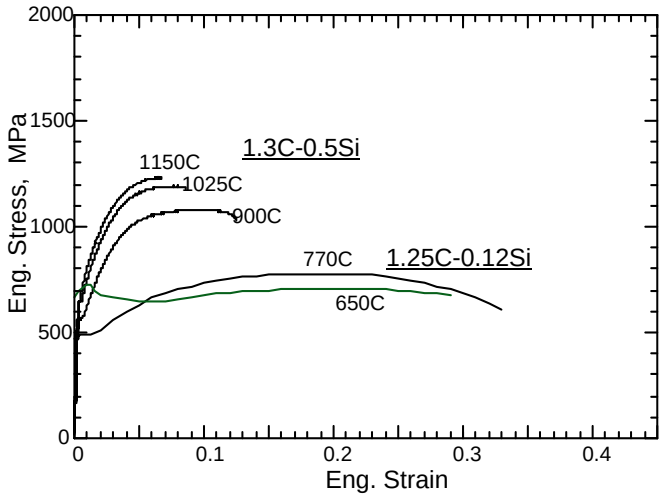

Fig. 6. Influence of extrusion temperature on the ambient temperature stress-strain response of UHCS alloys.

The influence of extrusion temperature on the ambient temperature stress-strain response is shown in Fig. 6 [10]. Data is provided for the UHCS-1.30C-0.5Si alloy and for a steel of related composition (UHCS-1.25C-.12Si). All materials were extruded at or above the A_1 temperature (750°C) with the exception of the extrusion at 650°C. The extrusion below the A_1 temperature resulted in a fully spheroidized structure, which had the highest yield strength but virtually no work hardening. The extrusions above the A_1 temperature resulted in fully-pearlitic or partially-pearlitic microstructures. For the extrusions at or above the A_1 temperature, the yield strength and work hardening rate increased with an increase in extrusion temperature. This trend is related to an increase in the amount of pearlite and a decrease in the interlamellar spacing in pearlite. The data in Fig. 6 dramatically illustrates the wide range of properties in extruded UHCS that can be obtained by changing the temperature of extrusion.

Figure 7 is a plot of the ultimate tensile strength as a function of elongation-to-failure for the extruded UHCS materials compared with dual phase, conventional high strength (HSLA), Inland's MartINsite steels and mild steels. As can be seen, the strength-ductility data for the as-extruded UHCSs fall in line with the dual-phase steels at strength levels from 500 to 1000 MPa. Very high strengths are achieved (>1250 MPa) with moderate elongations to failure (5 to 10%) for the as-extruded UHCSs. These results would classify the UHCSs as ultrahigh strength steels, with strength-ductility combinations approaching those exhibited by the MartINsite steels of Inland Steel.

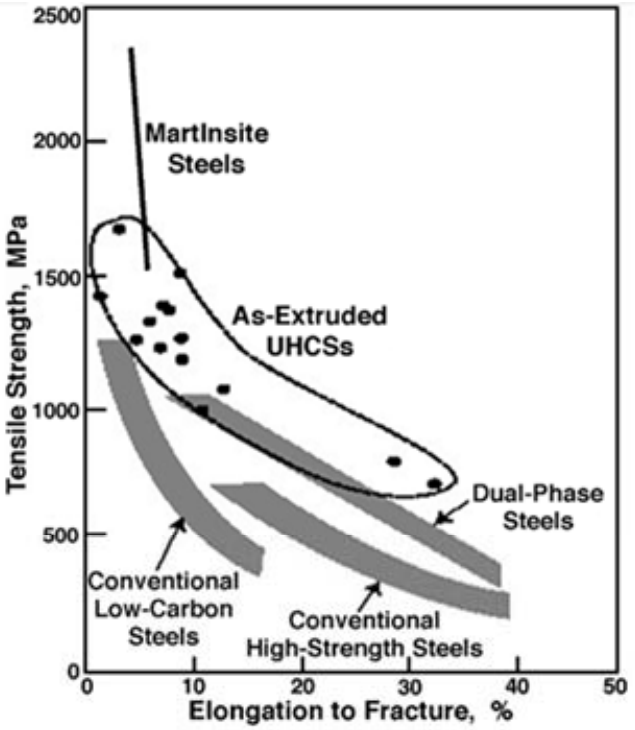

Fig. 7. Comparison of the ultimate tensile strength - elongation data for the as-extruded UHCS materials with dual phase, HSLA steels, mild steels and MartINsite steels.

Acknowledgements

The authors are indebted to Dan Whittenberger of NASA Glenn Research Center for extruding the UHCS materials. Work was performed under the auspices of the U.S. Department of Energy by the Lawrence Livermore National Laboratory under contract No. W-7405-ENG-48.

References

[1] D.R. Lesuer, C.K. Syn, A. Goldberg, J. Wadsworth and O.D. Sherby, J. Metals 45 (1993) 40-46.
[2] D.R. Lesuer, C.K. Syn, J.D. Whittenberger and O.D. Sherby, Metall. Mater. Trans. A 30A (1999) 1559-1568.
[3] D. R. Lesuer, C.K. Syn, J.D. Whittenberger and O.D. Sherby, accepted for publication in Int'l J. Plasticity (2000).
[4] J.J. Jonas and T. Chandra, in A.L. Hoffmanner (ed), Metal Forming: Interrelation Between Theory and Practice, Plenum, New York, 1971, pp. 115-129.
[5] O.D. Sherby and P.M. Burke, Prog. Mater. Sci. 13 (1968) 324-390.
[6] J. Weertman Trans. ASM 61 (1968) 681-694.
[7] D.R. Lesuer, C.K. Syn, J.D. Whittenberger, M. Carsi, O.S. Ruano and O.D. Sherby, accepted for publication in Materials Science and Eng. (2000).
[8] H.W. Mead and C.E. Birchenall, Trans. TMS-AIME 206 (1956) 1336-1339.
[9] C.W. Andrews, Metal Progress 58 (1950) 85-100.

[10] T. Oyama, C.K. Syn, D.R. Lesuer, J.D. Whittenberger and O.D. Sherby, in E.M. Taleff, C.K. Syn and D.R. Lesuer (eds), Deformation, Processing, and Properties of Structural Materials, TMS, Warrendale, PA, 2000, pp. 35-44.